Enhancement of terahertz coupling efficiency by improved antenna design in GaN/AlGaN high electron mobility transistor detectors*

Sun Yun-Fei(孙云飞)[a)b)c)d)], Sun Jan-Dong(孙建东)[a)c)], Zhang Xiao-Yu(张晓渝)[a)], Qin Hua(秦 华)[a)], Zhang Bao-Shun(张宝顺)[a)], and Wu Dong-Min(吴东岷)[a)b)†]

[a)] *International Laboratory for Adaptive Bio-Nanotechnology (i-Lab), Suzhou Institute of Nano-Technology and Nano-Bionics, Chinese Academy of Sciences, Suzhou* 215123, *China*

[b)] *Key Laboratory of Nanodevices, Suzhou Institute of Nano-Technology and Nano-Bionics, Chinese Academy of Sciences, Suzhou* 215123, *China*

[c)] *Graduate University of Chinese Academy of Sciences, Beijing* 100190, *China*

[d)] *College of Electronic & Information Engineering, Suzhou University of Science and Technology, Suzhou* 215011, *China*

(Received 9 February 2012; revised manuscript received 1 March 2012)

An optimized micro-gated terahertz detector with novel triple resonant antenna is presented. The novel resonant antenna operates at room temperature and shows more than a 700% increase in photocurrent response compared to the conventional bowtie antenna. In finite-difference-time-domain simulations, we found the performance of the self-mixing GaN/AlGaN high electron mobility transistor detector is mainly dependent on the parameters L_{gs} (the gap between the gate and the source/drain antenna) and L_w (the gap between the source and drain antenna). With the improved triple resonant antenna, an optimized micrometer-sized AlGaN/GaN high electron mobility transistor detector can achieve a high responsivity of 9.45×10^2 V/W at a frequency of 903 GHz at room temperature.

Keywords: terahertz detector, triple resonant antenna, two-dimensional electron gas, high electron mobility transistor

PACS: 85.60.Gz, 72.80.Ey, 85.35.Be, 84.40.Fe **DOI:** 10.1088/1674-1056/21/10/108504

1. Introduction

There are tremendous application potentials in terahertz (THz) detection devices. The THz detectors are widely used in different areas of spectroscopy and imaging. At present there is a large variety of THz detecting devices based on different principles and materials, such as a superconducting tunnel junction,[1] Ge and Si chip bolometers,[2] Schottky diodes that use semiconducting single-walled nanotubes,[3] carbon nanotube bolometers,[4] and quantum dot detectors.[5] These THz devices are either operated at low temperatures or with poor sensitivity. In recent years, detecting THz radiation with a room-temperature high electron mobility transistor (HEMT) has been actively pursued. It has been reported that there are possibilities of low production costs and excellent performance in THz detection, such as tunability,[6−11] operating at room temperature[12] and a relatively low value of the noise equivalent power.[13−15] In order to improve the performance of THz detectors, a great deal of attention has focused on the development of THz antennas for applications in THz detection technology, such as bowtie antenna,[16] rectangular microstrip patch antenna,[17] and other types of antennas.[18] Recently, Panasonic Corporation reported a resonant detection in a nanogate high electron mobility transistor. Using a gate-dipole antenna at room temperature, the device with a 80 nm-gate GaN/AlGaN high electron

*Project supported by the National Basic Research Program of China (Grant No. G2009CB929303), the Knowledge Innovation Program of the Chinese Academy of Sciences (Grant No. Y0BAQ31001), the National Natural Science Foundation of China (Grant Nos. 60871077 and 61107093), and the Visiting Professorship for Senior International Scientists of the Chinese Academy of Sciences (Grant No. 2010T2J07).

†Corresponding author. E-mail: dmwu2008@sinano.ac.cn

© 2012 Chinese Physical Society and IOP Publishing Ltd

mobility transistor offered a responsivity as high as 1.1×10^3 V/W.[19] Previously, our laboratory reported a THz detector with a triple resonant antenna and a low pass filter that could also reach a comparable responsivity.[20] As a very promising device for application in THz spectroscopy and imaging, the relationship between the detectors' responsivity and antenna geometry has not been fully studied. The purpose of the present work is to find an effective way to improve the performance of such triple resonant antenna high electron mobility transistor detectors.

2. Detection model and finite difference time domain simulations

The detection mechanism of a high electron mobility transistor device (as shown in Fig. 1) can be

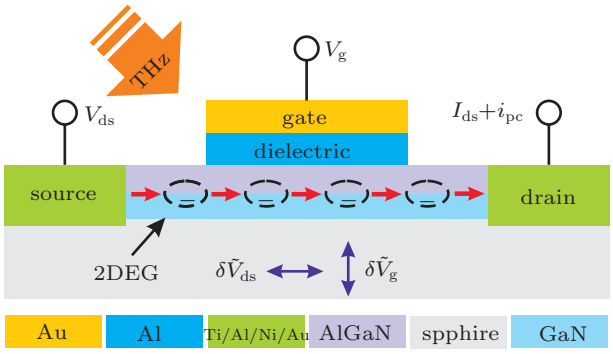


Fig. 1. (colour online) The schematic structure of the high electron mobility transistor detector based on the self-mixing mechanism.

explained by the self-mixing theory,[20–22] from which the photocurrent can be derived as

$$\begin{aligned} i_{\rm ds} &= \dot{G}(V_{\rm g})\delta V_{\rm g}\delta V_{\rm ds}\cos(\phi)/2 \\ &\propto \dot{G}(V_{\rm g})P_{\rm THz}, \end{aligned} \tag{1}$$

where

$$\begin{aligned} \dot{G}(V_{\rm g}) &= {\rm d}G/{\rm d}V_{\rm g} \\ &= {\rm d}^2 I_{\rm ds}/{\rm d}V_{\rm ds}{\rm d}V_{\rm g} \\ &\propto \mu W C_{\rm g}/L_{\rm g} \end{aligned}$$

is the derivative of conductance, $\delta V_{\rm ds}$ and $\delta V_{\rm g}$ are the incident THz wave induced horizontal and perpendicular electric potentials under the gate, ϕ is the phase shift between the two potentials, $P_{\rm THz}$ is the incident THz power, μ is the electron mobility, $C_{\rm g}$ is the capacitance between the Schottky gate and channel, and the width and length of gate are referred as W and $L_{\rm g}$, respectively.

It is clear that the self-mixing photocurrent is mainly dependent on the product of mixing fields ($E_xE_z\cos(\phi)$) under the gate and the derivative of conductance. Since the wavelength of THz radiation is much larger than the dimensions of the transistor channel, an antenna is necessary to provide coupling.

Figure 2(a) shows the schematic structures of a conventional bowtie antenna A and our newly designed triple resonant antenna B. The distribution of the perpendicular and horizontal electric field under the gates relevant to antennas A and B is confirmed by a finite-difference-time-domain (FDTD) simulation, as shown in Fig. 2(b). In our simulation, the frequency of the incident THz radiation was set as 900 GHz, and the wave vector of the incident THz wave is perpendicular to the surface of the antenna, while the polarization direction is parallel to the long axis of the antenna. From the simulation results in Fig. 2(b), we know that the distributions of the perpendicular and horizontal electric field enhancements (E_z and E_x) in the gap of antenna A are symmetrical, and they are very small under the gate due to the counteraction of the symmetrical electric charge induced by the THz wave, indicating that the conventional double-dipole antenna has a low coupling efficiency. To improve the perpendicular and horizontal electric fields, we replaced the gate pad with the gate antenna as shown in Fig. (2a)-B. Numerical simulations indicate that the triple resonant antenna produces a high THz electric field, and both the perpendicular and horizontal electric field enhancements under the gate of antenna A are far less than antenna B (E_x-A $\ll$ E_x-B and E_z-A $\ll$ E_z-B), and a strong mixing field factor

$$E_xE_z\cos(\phi) \simeq 6.8\times 10^3$$

is excited in the channel. This will ensure a good performance for the noise equivalent power (NEP) and response of our detector. The characterization will be detailed in the following sections.

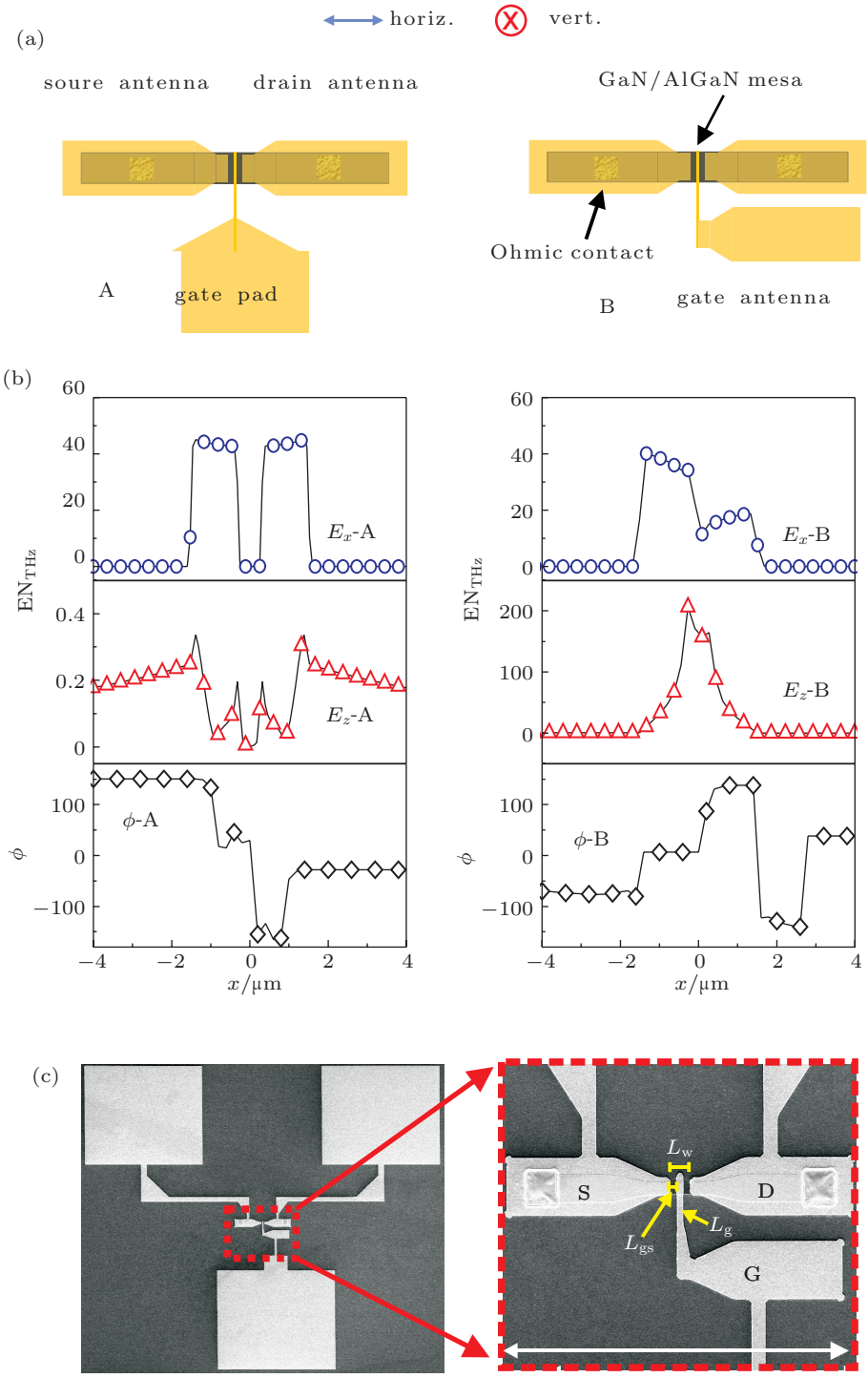


Fig. 2. (colour online) (a) The schematic structures of conventional bowtie antenna A and our designed triple resonant antenna B. (b) Distribution of the induced electric fields and phase shift between E_x and E_z in the gap of antennas A and B, respectively. (c) The scanning electron microscope graph of the detector.

3. Experiments and results

In this study, six different detectors with similar antenna based on a GaN/$Al_{0.27}Ga_{0.73}N$ heterostructure were fabricated and measured in order to find an effective way to optimize our HEMT mixer. The two-dimensional electron gas (2DEG) about 33 nm below the surface has an electron mobility of 1400 cm^2/Vs and an electron density of 1.3×10^{13} cm^{-2} at room temperature. The first four devices (defined as # 1,

2, # 3, and # 4) have the same gate length of $L_g = 2$ μm and a different distance between the source and drain antennas ($L_w = 7$ μm, 6 μm, 5 μm, and 4 μm for # 1 to # 4, respectively), the other two detectors (defined as # 5, # 6) have the same source-to-drain antenna distance of $L_w = 4$ μm and different gate length of $L_g = 1$ μm and 0.5 μm, respectively. In addition, the sensor properties of a similar HEMT detector without the gate antenna was also fabricated and tested as a comparison. The scanning electron microscope graph and a zoom-in view of # 1 are shown in Fig. 2(c). The source, drain, and gate electrodes integrated with a resonant antenna are extended to a gold pad (200 μm × 200 μm). The gap between the gate and the right/left antenna is 2.5 μm.

We have used the same experimental setup for THz radiation detection as described in our previous work.[20,21] The differential conductance $G = \mathrm{d}I_{ds}/\mathrm{d}V_{ds}$ versus gate voltage (V_g) for different samples measured at 300 K are shown in Fig. 3(a). Without THz radiation, the two-dimensional electron gas (2DEG) under the gate can be pinched off completely at $V_g \leq -4.0$ V, and fully opened when $V_g \geq -2.5$ V for samples # 1, # 2, # 3, and # 4. The threshold voltages are shifted by about 0.5 V for nano-gate samples # 5 and # 6 due to the process of electron beam lithography. The corresponding derivative of channel conductance, $\mathrm{d}G/\mathrm{d}V_g$, are also shown in Fig. 3(b). When the THz wave at 903 GHz is on, a strong direct photocurrent (i_{ds}) is induced when the electron channel is strongly modulated by the gate voltage, as shown in Fig. 3(c). The peak response in photocurrent and the maximum of $\dot{G}(V_g)$ are located at the same position, consistent with the self-mixing detection mechanism. The photocurrent is reduced to zero when the electron channel is completely turned off. From the measured photocurrent results, we can easily obtain that (i) the photocurrent can be improved from 3.2 nA to 13.3 nA by decreasing L_w from 7 μm to 4 μm when $L_g = 2$ μm; (ii) the increasing of the gate length from 0.5 μm to 2 μm results in a photocurrent improvement from 9.1 nA to 13.3 nA. In other words, the shorter L_w and L_{ds} promise a higher response. The product of the mixing fields in the 2DEG for these six samples were simulated and plotted as shown in Figs. 3(d) and 3(e), which coincide with the measured photocurrent for our HEMT detectors. This result is different from the opposite tendency reported by the Panasonic Corporation. The point view of their plasmon-resonant detection is that the device with a shorter gate length apparently exhibits better responsivity. The principal cause of such difference is due to the different detection mechanisms.

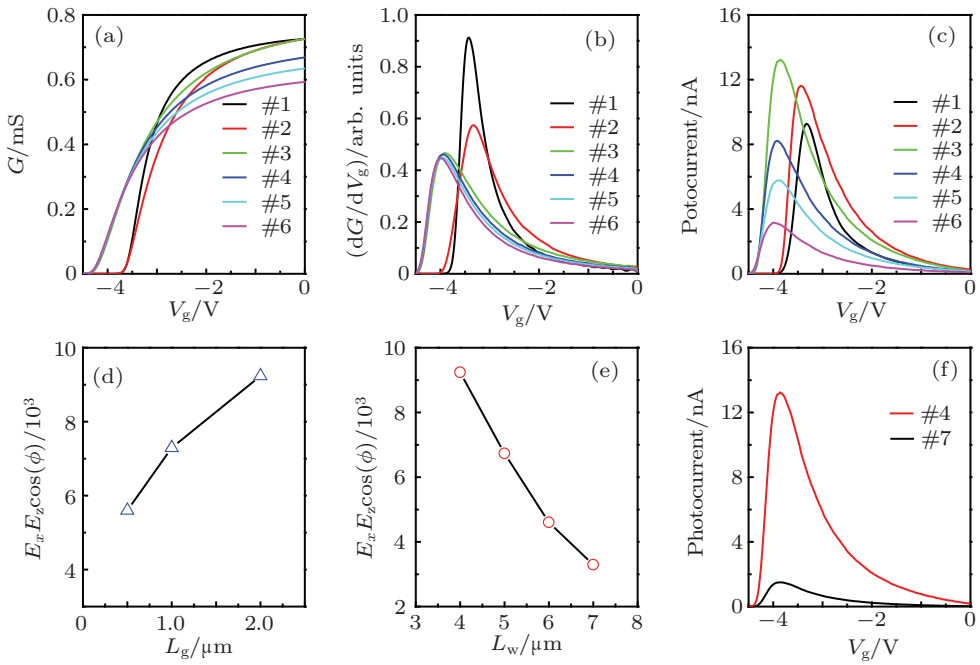


Fig. 3. (colour online) (a) The channel conductance which was modulated by the gate voltage at 300 K. (b) The measured source–drain derivative of the channel conductance. (c) The experimental photocurrent as a function of the gate voltage. Panels (d) and (e) are the mixing factor $E_x E_z \cos(\phi)$ from an FDTD simulation at 903 GHz. (f) The measured photocurrent for HEMT detectors with triple resonant antenna and conventional bowtie antenna.

For comparison, we have made a control device # 7 (without gate antenna) with identical antenna, gate length, source–drain distance, and bonding pads such as # 4 (with gate antenna). Both devices have the same direct current (DC) electrical characteristics. However, the photocurrent of the detector with the bowtie antenna is much smaller than the detector with the gate antenna, and the triple resonant antenna caused a 700% increase in the measured photocurrent. This result indicates that the triple resonant antenna can effectively receive the incoming THz wave and enhance the self-mixing factor in the 2DEG channel which gives rise to a significant increase in photocurrent. The electric and optical characteristics based on the model described above are summarized in Table 1. The responsivity of the HEMT detector is found to be crucially dominated by the size of $L_{\rm w}$ and $L_{\rm gs}$. The optimization of the HEMT detectors resulted in an improvement in the photo-voltage from 258 V/W to 945 V/W and an improvement in the noise equivalent power (NEP) from 9.4×10^{-11} W/$\sqrt{\rm Hz}$ to 2.8×10^{-11} W/$\sqrt{\rm Hz}$ at a frequency of 903 GHz at 300 K. We also measured the polarization-dependent THz response of device # 4. The orientation parallel to the antenna length is defined as 0° or 180°. The maximum response was observed when the polarization was along the length of the antennas as shown in Fig. 4(a). In Fig. 4(b), we present two-dimensional images obtained with a radiation above 1 THz at room temperature. The image clearly reveals the objects including the key, coin, paperclip, and watches sealed in the envelope.

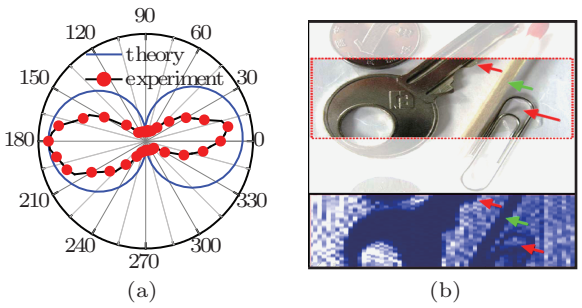


Fig. 4. (colour online) (a) The amplitude of the photovoltaic signal for 937 GHz Versus the polarization angle. (b) A raster-scan image taken at 1024 GHz and a modulation frequency of 706 Hz. All data are taken at 300 K.

Table 1. Measured characteristics for different samples at 300 K.

Samples #	$L_{\rm w}/L_{\rm g}$	$L_{\rm w}/L_{\rm gs}$	G/mS	(dG/d$V_{\rm g}$)/(mS/V)	$P_{\rm c}$/nA	I_n/A	R_i/(mA/W)	R_v/(V/W)	NEP/(W/Hz$^{0.5}$)
1	7/2	7/2.5	0.05	0.45	3.2	1.22×10^{-12}	12.9	258	9.4×10^{-11}
2	6/2	6/2	0.052	0.46	5.9	1.34×10^{-12}	23.9	459	5.6×10^{-11}
3	5/2	5/1.5	0.055	0.47	8.2	1.46×10^{-12}	33.2	603	4.3×10^{-11}
4	4/2	4/1	0.057	0.48	13.3	1.52×10^{-12}	53.9	945	2.8×10^{-11}
5	4/1	4/1.5	0.06	0.57	11.5	1.67×10^{-12}	46.6	776	3.5×10^{-11}
6	4/0.5	4/1.75	0.07	0.91	9.1	1.72×10^{-12}	36.9	527	4.6×10^{-11}
7	4/2	4/1	0.057	0.48	1.9	1.52×10^{-12}	7.7	110	2.4×10^{-10}

4. Conclusions

In conclusion, the triple resonant antenna was shown to have excellent performance for self-mixing HEMT THz detectors compared to a conventional bowtie antenna. By comparing the measured photocurrent of different devices, we found that a decrease of $L_{\rm w}$ and $L_{\rm gs}$ resulted in a 366% and 179% improvement in the response, respectively, giving us a useful method to design THz antenna rationally. Perhaps the most important elements such as the carrier density and the non-uniform THz fields under the gate play an important role for the detection efficiency. Many questions remain to be answered, and in future work we will fabricate and test focal plan detector arrays by integrating read-out circuits with the array.

Acknowledgement

The authors gratefully thank Dr. Cai Yong and Dr. Lu Min for their instructive suggestions throughout our experiments. We thank Dr. Dawson for helping us improve the English of our paper thoroughly.

References

[1] Nahum M and Martinis John M 1993 *Appl. Phys. Lett.* **63** 3075

[2] Richard P L 1994 *J. Appl. Phys.* **76** 12

[3] Manohara H M, Wong E W, Schlecht E, Hunt B D and Siegel P H 2005 *NanoLett.* **5** 1469

[4] Tarasov M, Svensson J, Weis J, Kuzmin L and Campbell E 2006 *JETP Lett.* **84** 267

[5] Kawano Y, Fuse T, Toyokawa S, Uchida T and Ishibashi K 2008 *J. Appl. Phys.* **103** 034307

[6] Lü J Q and Shur M S 2001 *Appl. Phys. Lett.* **78** 2587

[7] Knap W, Deng Y, Rumyantsev S and Shur M S 2002 *Appl. Phys. Lett.* **81** 4637

[8] Otsuji T, Hanabe M and Ogawara O 2004 *Appl. Phys. Lett.* **85** 2119

[9] Fatimy A El, Teppe F, Dyakonova N, Knap W, Seliuta D, Valušis G, Shchepetov A, Roelens Y, Bollaert S, Cappy A and Rumyantsev S 2006 *Appl. Phys. Lett.* **89** 131926

[10] Ryzhii V, Ryzhii M, Hu Y, Hagiwara I and Shur M S 2007 *Appl. Phys. Lett.* **90** 203503

[11] Ma M R, Chen Y L, Wang L M and Wang C 2008 *Chin. Phys.* B **17** 1854

[12] Teppe F and Knap W 2005 *Appl. Phys. Lett.* **87** 052107

[13] Tauk R, Teppe F, Boubanga S, Coquillat D, Knap W, Meziani Y M, Gallon C, Boeuf F, Skotnicki T, Fenouillet-Beranger C, Maude D K, Rumyantsev S and Shur M S 2006 *Appl. Phys. Lett.* **89** 253511

[14] Fatimy A El, Boubanga Tombet S, Teppe F, Knap W, Veksler D B, Rumyantsev S, Shur M S, Pala N, Gaska R, Fareed Q, Hu X, Seliuta D, Valusis G, Gaquiere C, Theron D and Cappy A 2006 *Electron. Lett.* **42** 1342

[15] Zhou J J, Jiang R L, Sha J, Liu J, Shen B, Zhang R and Zheng Y D 2003 *Chin. Phys.* **12** 785

[16] Shitov S V, Jackson B D, Baryshev A M, Markov A V, Iosad N N, Gao J R and Klapwijk T M 2002 *Physica* C **372** 374

[17] Sundararajan B, Kazuomi E, Tadao T and Yutaka O 2010 *Solid-State Electronics* **54** 1578

[18] Kim S, Jeramy D Z, Paolo F, Gossard A C, Wu D H and Sherwin M S 2008 *Appl. Phys. Lett.* **92** 253508

[19] Tanigawa T, Onishi T, Takigawa S and Otsuji T 2010 *Device Research Conference at South Bend*, IN, June 22 p. IV.A-9

[20] Sun Y F, Sun J D, Zhou Y, Tan R B, Zeng C H, Xue W, Qin H, Zhang B S and Wu D M 2011 *Appl. Phys. Lett.* **98** 252103

[21] Sun J D, Sun Y F, Wu D M, Cai Y, Qin H and Zhang B S 2012 *Appl. Phys. Lett.* **100** 1013506

[22] Öjefors E, Lisauskas A, Glaab D, Roskos H G and Pfeiffer U R 2009 *J. Infrared Milli. Terahz. Waves* **30** 1269